Computational Thermal Sciences, 13(2):21–43 (2021)

EFFECTS OF VARIABLE THERMAL CONDUCTIVITY OF WATER-BASED NANOFLUIDS SATURATED WITH POROUS MEDIUM ON NATURAL CONVECTION HEAT TRANSFER ENHANCEMENT

J.C. Umavathi,[1] Ali Al-Mudhaf,[2] & Ali J. Chamkha[3,]*

[1]*Department of Mathematics, Gulbarga University, Gulbarga-585 106, Karnataka, India*
[2]*Manufacturing Engineering Department, The Public Authority for Applied Education and Training, Shuweikh 70654, Kuwait*
[3]*Kuwait College of Science and Technology, Doha District, Kuwait*

*Address all correspondence to: Ali J. Chamkha, Faculty of Engineering, Kuwait College of Science and Technology, 7th Ring Road, Doha District, Kuwait, E-mail: a.chamkha@kcst.edu.kw

Original Manuscript Submitted: 8/25/2020; Final Draft Received: 9/5/2020

In this work, the natural convection fluid flow and heat transfer in a vertical rectangular duct filled with nanofluids and saturated with a porous medium was investigated numerically. The non-Darcy model was used to define the porous matrix. Water was used as the base fluid with different types of nanoparticles, such as copper, titanium oxide, silver, and diamond. The flow was considered to be laminar and fully developed, the thermal conductivity was assumed to vary linearly with the temperature, and the viscosity was assumed to be constant with the temperature. The two-dimensional Navier—Stokes and energy equations were solved simultaneously using the finite-difference method. The effect of the fluid flow and heat transfer characteristics, such as the velocity, temperature, volumetric flow rate, skin friction, and rate of heat transfer distribution in the duct, was investigated. The results showed that the flow accelerates with an increase in the variable thermal conductivity parameter, Grashof number, Brinkman number, and aspect ratio, whereas the inertial parameter and solid volume fraction decelerates the flow. The rate of heat transfer increased for the nanofluid when compared to the regular fluid for all of the nanoparticles considered in the study.

KEY WORDS: *natural convection, nanofluids, variable thermal conductivity, viscous dissipation, rectangular duct, finite-difference method*

1. INTRODUCTION

Buoyancy-driven fluid flow and heat transfer in ducts are encountered in a number of industrial applications such as heat exchangers, home ventilation systems, and electronic cooling devices. Low thermal conductivity of conventional fluids such as water, engine oil, and ethylene glycol oil is a heat transfer drawback in heat exchangers. Solids have larger thermal conductivity; therefore, dispersing them in fluids can help to improve their thermal characteristics. Fluids that contain suspended nanoparticles such as metals or oxides are called nanofluids. It has been noted that no sedimentation occurs since nanoscale particles are kept suspended in the base fluid. Similarly, no significant increase in the pressure drop within the flow field takes place. Investigations have revealed that nanofluids exhibit enhanced thermal properties compared to the base fluids; and therefore, they have attracted attention as a new generation of heat transfer fluids in plants, heat exchangers, building heating systems, and automobile cooling devices because of their excellent thermal performance (Choi, 1995). For example, it has been reported that a very small amount (less than 1% in terms of the volume fraction) of copper nanoparticles can improve the measured thermal conductivity of the suspension by 40% (Lee et al., 1999; Eastman et al., 2001), and over 150% improvement of the effective

NOMENCLATURE

A	aspect ratio (b/a)
a	horizontal distance
b	vertical distance
BK	variable conductivity parameter $(c\Delta T)$
Br	Brinkman number $\left[=\mu_f^3/\left(K_0\Delta T\rho_f^2 b^2\right)\right]$
c	empirical constant
Da	Darcy number $\left(\kappa/b^2\right)$
Gr	Grashof number $\left(=g\beta_f\Delta T\, b^3\rho_f^2/\mu_f^2\right)$
I	inertial parameter $\left(=C_F\, b/\sqrt{\kappa}\right)$
K	conductivity of the fluid
Nx, Ny	grid number in computational domain
T	temperature
T_0	reference temperature
U, V, W	velocity components
u, v, w	dimensionless velocity components
X, Y, Z	space coordinates
x, y, z	dimensionless space coordinates

Greek Symbols

θ	dimensionless temperature
κ	permeability of the porous medium
μ	viscosity
ρ	density
ϕ	solid volume fraction

Subscripts

nf	thermo-physical properties of the nanofluids
f	base fluid
s	solid nanoparticles

thermal conductivity at a volume fraction of 1% was reported by Choi et al. (2001) for multi-walled carbon nanotubes suspended in oil. Pak and Cho (1998) measured the convective heat transfer coefficient with nanoparticles of γ-Al_2O_3 and TiO_2 dispersed in water. Their experimental results revealed that the heat transfer coefficients of the nanofluids increased with increasing volume fraction of the nanoparticles and Reynolds number. Their heat transfer data showed Nusselt numbers up to 30% higher than predicted by the pure liquid correlation. Recently, Umavathi et al. (2015) analyzed the convective heat transfer in a vertical rectangular duct filled with a nanofluid.

Fluid flow and transport processes through porous structures constitute a topic of great interest in various scientific and technical fields. In particular, in engineering applications such as catalytic converters (used to reduce toxicity and exhaust emissions from automobiles engines), condensers (used as heat exchangers for cooling condensers), and gas turbines (used to cool gas turbine blades), fluid flow through porous media in the high-velocity regime becomes relevant. The Austrian scientist, Forchheimer (1901), investigated fluid flow through porous media in the high-velocity regime and observed that as the flow velocity increases, the inertial effects start to dominate the flow. In order to account for these high-velocity inertial effects, he suggested including an inertial term representing the kinetic energy of the fluid in the Darcy equation (Darcy, 1856). Holditch and Morse (1976) numerically investigated the non-Darcy effect on effective fracture conductivity and gas well productivity. Their results showed that at the near-wellbore region, non-Darcy flow could reduce the effective fracture conductivity by a factor of 20 or more, and gas productivity by 50%. Non-Darcy behavior has shown significant influence on well performance. Umavathi and Santosh (2012) studied the mixed convection in a vertical channel for Robin boundary conditions using the Forchheimer model. The effects of the source and sink were analyzed by Umavathi et al. (2012) using the Forchheimer model. A detailed explanation of different porous media models is given in Umavathi (2013a).

Many studies have been conducted on heat transfer in porous media with nanofluids to predict the effects of the porous media and nanofluids characteristics on natural, forced, and mixed convection heat transfer. These studies have shown that the convection heat transfer increased when porous media are filled with high thermal conductivity nanofluids and that this increase depended on the nanofluid type. Hashemi Amerei and Dehkordi (2014) studied mixed-convection in vertical porous and regular channels for both regular fluids and nanofluids, taking into account influence of viscous heating and inertial force. Mittal et al. (2013) numerically studied the mixed convection in a lid-driven porous cavity saturated by nanofluids. Their findings indicated that the addition of nanoparticles to a

base fluid augmented the heat transfer coefficient and was found to significantly increase with an increase in the particle volume concentration. A constant volume fraction and higher value of the Grashof number, with an increase in the Darcy number, increased the average Nusselt number. Nield and Kuznetsov (2009) analytically studied the onset of free convection heat transfer in a horizontal layer of a porous medium filled with nanofluids. The effects of thermophoresis and Brownian motion on heat transfer were investigated. Following the work of Nield and Kuznetsov (2009), Umavathi (2013b, 2015a) studied the effect of thermal modulation on the onset of convection using nanofluids and Umavathi and Mohite (2014a,b) studied the effect of cross diffusion for variations of viscosity and conductivity on the stability of nanofluids saturated with porous medium.

Almost all of the aforementioned studies have assumed that the fluid properties are constant. However, it is known that the physical properties of the fluid may change significantly when exposed to temperature. In industrial systems, fluids can be subjected to extreme conditions such as high temperatures, pressure, high shear rates, and external heating and each of these factors can lead to high temperatures being generated within the fluid. For example, the viscosity of glycerin has a threefold decrease in magnitude for a 10°C rise in temperature (Harms et al., 1998). This trend has been observed not only in such viscous liquids but also in other liquids such as water, where the viscosity of the water decreases by about 240% when the temperature increases from 10°C to 50°C, as reported by Ling and Dybbs (1992). As a result, the constant property solutions most often given in the literature need to be modified. Viscosity variation with temperature in the case of fluids clear of solid material has been the subject of many studies thus far and a complete literature survey may be found in Kays and Crawford (1993). According to Anyakoha (2010), Batchelor (1987), Meyers et al. (2006), and other researchers of fluid dynamics, it is a well-known fact that the properties most sensitive to temperature rise are viscosity and thermal conductivity. Recently, Umavathi and her team (Astaninal et al., 2015; Umavathi, 2015a,b; Umavathi and Sheremet, 2016) studied variable properties on convection flow for various fluids.

The main objective of the present study was to investigate the free-convective flow of a viscous incompressible fluid in porous medium saturated with nanofluid in a vertical rectangular duct, in which the thermal conductivity is considered to be dependent on temperature and the viscosity is considered to be constant with temperature. Numerical solutions are discussed with graphical representations.

2. MATHEMATICAL FORMULATION

Figure 1 shows a schematic diagram of a differentially heated enclosure. The height and width of the duct are given by b and a, respectively. The aspect ratio is defined as the ratio of the height to the width of the enclosure ($A = b/a$). In this study, the left wall was heated and maintained at a constant temperature (T_1) that was lower than the right wall temperature (T_2). The other two sides of the duct were set at $\partial T/\partial X = 0$. The fluid in the enclosure was a nanofluid saturated with a porous medium. Water was used as the base fluid and copper, titanium oxide, silver, and diamond were

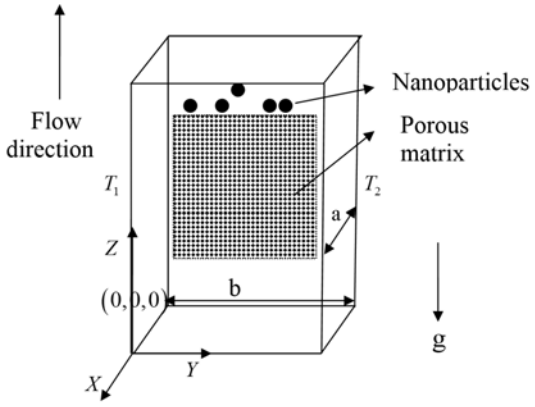

FIG. 1: Physical configuration

used as the nanoparticles. The nanofluid was assumed to be incompressible and the flow was conceived as laminar and two-dimensional. It was presumed that the mixture of water and nanoparticles was in thermal equilibrium and no slip occurred between the two media. The density variation in the nanofluid was approximated using the standard Boussinesq model. The viscosity was assumed to be constant with the temperature, whereas the thermal conductivity was assumed to be linearly dependent on the temperature. Furthermore, in the present study, it was also presumed that the temperature of the fluid phase was equal to the temperature of the porous solid matrix everywhere and the local thermal equilibrium was valid. The porous medium was considered to be homogeneous and isotropic. The non-Darcian model, taking into account the effects of inertial forces and viscous and Darcy dissipations, was employed in defining the model.

Taking into account the aforementioned assumptions, the governing equations for the laminar, steady-state natural convection are given as follows:

$$\mu_{\mathrm{nf}}\left(\frac{\partial^2 W}{\partial X^2}+\frac{\partial^2 W}{\partial Y^2}\right)+g\left(\rho\beta\right)_{\mathrm{nf}}\left(T-T_0\right)-\frac{\mu_{\mathrm{nf}}}{\kappa}W-\frac{\rho_{\mathrm{nf}}C_F}{\sqrt{\kappa}}W^2=0 \tag{1}$$

$$\frac{\partial}{\partial X}\left(K_{\mathrm{nf}}\frac{\partial T}{\partial X}\right)+\frac{\partial}{\partial Y}\left(K_{\mathrm{nf}}\frac{\partial T}{\partial Y}\right)\frac{\partial T}{\partial Y}+\mu_{\mathrm{nf}}\left[\left(\frac{\partial W}{\partial X}\right)^2+\left(\frac{\partial W}{\partial Y}\right)^2\right]+\frac{\mu_{\mathrm{nf}}}{\kappa}W^2=0 \tag{2}$$

Equations (1) and (2) are solved subjected to the following boundary conditions:

$$\begin{aligned}
&W=0,\quad T=T_1 \quad \text{at} \quad Y=0 \quad \text{for} \quad 0\le X\le a\\
&W=0,\quad T=T_2 \quad \text{at} \quad Y=b \quad \text{for} \quad 0\le X\le a\\
&W=0,\quad \frac{\partial T}{\partial X}=0 \quad \text{at} \quad X=0 \quad \text{for} \quad 0\le Y\le b\\
&W=0,\quad \frac{\partial T}{\partial X}=0 \quad \text{at} \quad X=a \quad \text{for} \quad 0\le Y\le b
\end{aligned} \tag{3}$$

The thermal diffusivity is written as follows:

$$\alpha_{\mathrm{nf}}=\frac{K_{\mathrm{nf}}}{\left(\rho C_p\right)_{\mathrm{nf}}} \tag{4}$$

Also, the effective density of the nanofluid is given by:

$$\rho_{\mathrm{nf}}=\left(1-\phi\right)\rho_{\mathrm{f}}+\phi\,\rho_{\mathrm{s}} \tag{5}$$

where ϕ is the solid volume fraction of the nanoparticles.

The heat capacitance and thermal expansion coefficients are expressed as follows:

$$\left(\rho C_p\right)_{\mathrm{nf}}=\left(1-\phi\right)\left(\rho C_p\right)_{\mathrm{f}}+\phi\left(\rho C_p\right)_{\mathrm{s}} \tag{6}$$

$$\left(\rho\beta\right)_{\mathrm{nf}}=\left(1-\phi\right)\left(\rho\beta\right)_{\mathrm{f}}+\phi\left(\rho\beta\right)_{\mathrm{s}} \tag{7}$$

The effective dynamic viscosity of the nanofluid given by Brinkman (1952) is:

$$\mu_{\mathrm{nf}}=\frac{\mu_{\mathrm{f}}}{\left(1-\phi\right)^{2.5}} \tag{8}$$

In Eq. (4), K_{nf} is the thermal conductivity of the nanofluid. According to Maxwell (1904), this equation for spherical nanoparticles can be written as follows:

$$K_{\mathrm{nf},0}=K_{\mathrm{f}}\frac{K_{\mathrm{s}}+2K_{\mathrm{f}}-2\phi\left(K_{\mathrm{f}}-K_{\mathrm{s}}\right)}{K_{\mathrm{s}}+2K_{\mathrm{f}}+\phi\left(K_{\mathrm{f}}-K_{\mathrm{s}}\right)} \tag{9}$$

where subscripts nf, f, and s are the thermophysical properties of the nanofluids, base fluid, and solid nanoparticles, respectively. The thermal conductivity of the nanofluid is assumed to vary with temperature as $K_{\mathrm{nf}}=K_{\mathrm{nf},0}f\left(T\right)$.

Function f is linearly dependent on temperature as $f(T) = 1 + c(T - T_0)$, where parameter c is negative or positive depending on the type of fluid under study.

The following dimensionless variables are introduced to the non-dimensional governing equations given by Eqs. (1) and (2) along with the boundary conditions given in Eq. (3):

$$\begin{aligned} &x = X/b, \quad y = Y/b, \quad w = (W\rho_f b)/\mu_f, \quad \theta = (T - T_0)/(T_2 - T_1), \quad T_0 = (T_1 + T_2)/2 \\ &\mathrm{Gr} = \left(g\,\beta_f\,\Delta T\,b^3\rho_f^2\right)/\mu_f^2, \quad \mathrm{Br} = \mu_f^3/\left(K_0\,\Delta T\,\rho_f^2 b^2\right), \quad \mathrm{Da} = \kappa/b^2, \quad I = (C_F\,b)/\sqrt{\kappa}, \quad BK = c\,\Delta T \end{aligned} \tag{10}$$

where subscript 0 stands for the reference temperature. The governing equations in dimensionless form are given as follows:

$$\frac{\partial^2 w}{\partial x^2} + \frac{\partial^2 w}{\partial y^2} + (1-\phi)^{2.5}\left[(1-\phi) + \phi\frac{(\rho\beta)_s}{(\rho\beta)_f}\right]\mathrm{Gr}\theta - \frac{w}{\mathrm{Da}} - I\,(1-\phi)^{2.5}\left[(1-\phi) + \phi\,\frac{\rho_s}{\rho_f}\right]w^2 = 0 \tag{11}$$

$$\begin{aligned} &\frac{\partial^2\theta}{\partial x^2} + \frac{\partial^2\theta}{\partial y^2} + \frac{BK}{(1+BK\theta)}\left[\left(\frac{\partial\theta}{\partial x}\right)^2 + \left(\frac{\partial\theta}{\partial y}\right)^2\right] + \frac{\mathrm{Br}\,kr}{(1-\phi)^{2.5}\,(1+BK\theta)}\left[\left(\frac{\partial w}{\partial x}\right)^2 + \left(\frac{\partial w}{\partial y}\right)^2\right] \\ &+ \frac{\mathrm{Br}\,kr}{\mathrm{Da}\,(1-\phi)^{2.5}\,(1+BK\theta)}w^2 = 0 \end{aligned} \tag{12}$$

where

$$kr = \left[\frac{K_s + 2K_f + \phi\,(K_f - K_s)}{K_s + 2K_f - 2\phi\,(K_f - K_s)}\right]$$

The corresponding non-dimensional boundary conditions used to solve Eqs. (11) and (12) become:

$$\begin{aligned} &w = 0, \quad \theta = -0.5 \quad \text{at} \quad y = 0 \quad \text{for} \quad 0 \le x \le A \\ &w = 0, \quad \theta = 0.5 \quad \text{at} \quad y = 1 \quad \text{for} \quad 0 \le x \le A \\ &w = 0, \quad \frac{\partial\theta}{\partial x} = 0 \quad \text{at} \quad x = 0 \quad \text{and} \quad x = A \quad \text{for} \quad 0 \le y \le 1 \end{aligned} \tag{13}$$

3. SOLUTION METHOD

The Navier—Stokes equations governing the flow model as given in Eqs. (12) and (13) along with boundary conditions (13) cannot be solved in closed form owing to their coupled, nonlinear, and two-dimensional nature. Therefore, we resorted to finding approximate solutions using numerical techniques. We adopted the well-known finite-difference method. The solution procedure consisted of discretizing the second derivative and the squared first derivatives using the central difference of second-order accuracy. After applying the finite differences, the reduced difference equations along with the boundary conditions are as follows:

$$\begin{aligned} &\frac{w_{i+1,j} - 2w_{i,j} + w_{i-1,j}}{\Delta x^2} + \frac{w_{i,j+1} - 2w_{i,j} + w_{i,j-1}}{\Delta y^2} + (1-\phi)^{2.5}\left[(1-\phi) + \phi\frac{(\rho\beta)_s}{(\rho\beta)_f}\right]\mathrm{Gr}\theta_{i,j} \\ &- \frac{w_{i,j}}{\mathrm{Da}} - (1-\phi)^{2.5}\left[(1-\phi) + \phi\frac{(\rho\beta)_s}{(\rho\beta)_f}\right]w_{avj}w_{i,j} = 0 \end{aligned} \tag{14}$$

$$\begin{aligned} &\frac{\theta_{i+1,j} - 2\theta_{i,j} + \theta_{i-1,j}}{\Delta x^2} + \frac{\theta_{i,j+1} - 2\theta_{i,j} + \theta_{i,j-1}}{\Delta y^2} + \frac{BK}{(1+BK\theta)}\left[\left(\frac{\theta_{i+1,j} - \theta_{i-1,j}}{2\Delta x}\right)^2\right. \\ &\left. + \left(\frac{\theta_{i,j+1} - \theta_{i,j-1}}{2\Delta y}\right)^2\right]\frac{\mathrm{Br}\,kr}{(1-\phi)^{2.5}\,(1+BK\theta)}\left[\left(\frac{w_{i+1,j} - w_{i-1,j}}{2\Delta x}\right)^2 + \left(\frac{w_{i,j+1} - w_{i,j-1}}{2\Delta y}\right)^2\right] \\ &+ \frac{\mathrm{Br}\,kr}{\mathrm{Da}\,(1-\phi)^{2.5}\,(1+BK\,\theta)}w_{i,j}^2 = 0 \end{aligned} \tag{15}$$

$$\begin{aligned} w_{i,0} &= -w_{i,1}, & \theta_{i,0} &= -1-\theta_{i,1} \\ w_{i,Ny+1} &= -w_{i,Ny}, & \theta_{i,Ny+1} &= 1-\theta_{i,Ny} \\ w_{0,j} &= -w_{1,j}, & \theta_{0,j} &= \theta_{1,j} \\ w_{Nx+1,j} &= -w_{Nx,j}, & \theta_{Nx+1,j} &= \theta_{Nx,j} \end{aligned} \tag{16}$$

where i and j range from 1 to Nx and 1 to Ny, respectively, in which Nx and Ny denote the number of grids inside the computational domain in the x-and y-directions, respectively. With the given pertinent parameters, the values of $w_{i,j}$ and $\theta_{i,j}$, after setting boundary conditions (16), are iterated according to difference Eqs. (14) and (15). Until all of the values of $w_{i,j}$ and $\theta_{i,j}$ in the grid system are less than a prescribed tolerance, the solutions are assumed to be sought.

The computational domain was divided into 100 grids in the y-direction and $100 \times A$ grids in the x-direction. The solutions were obtained when all of the elements in the grids were less than 10^{-14} after a suitable number of iterations. The validity of the scheme was done through a grid independent study, and the iteration process was terminated when the solutions on the 100×100 and 160×160 grids were almost same.

4. RESULTS AND DISCUSSION

In this section, a representative set of graphical results are presented to illustrate the influence of various physical parameters on the heat transfer characteristics in the cavity. Water was used as the base fluid in combination with different nanoparticles. The ranges of the magnitude of the variable thermal conductivity parameter, Darcy number, inertial parameter, Grashof number, Brinkman number, solid volume fraction, and aspect ratio used in this study were $-1.0 \le BK \le 1.0$, $0.0001 \le \mathrm{Da} \le 1.0$, $0.0 \le I \le 10$, $1 \le \mathrm{Gr} \le 25$, $0.01 \le \mathrm{Br} \le 2$, $0.0 \le \phi \le 0.05$, and $0.5 \le \mathrm{A} \le 2.0$, respectively, for different nanoparticles. The graphs were drawn using the MATLAB software program and viewed in three, two, and one dimensions in order to better understand the flow. The one-dimensional graphs were plotted in the midsection of the duct at $y = 0.5$ for variations of x $(0 \le x \le 1)$.

Figure 2(a) presents contour maps of the velocity and temperature in a square cavity $(A = 1)$ using different nanoparticles for the variations of BK $(-0.5 \le BK \le 0.5)$. It can be seen from Fig. 2(a) that the number of velocity

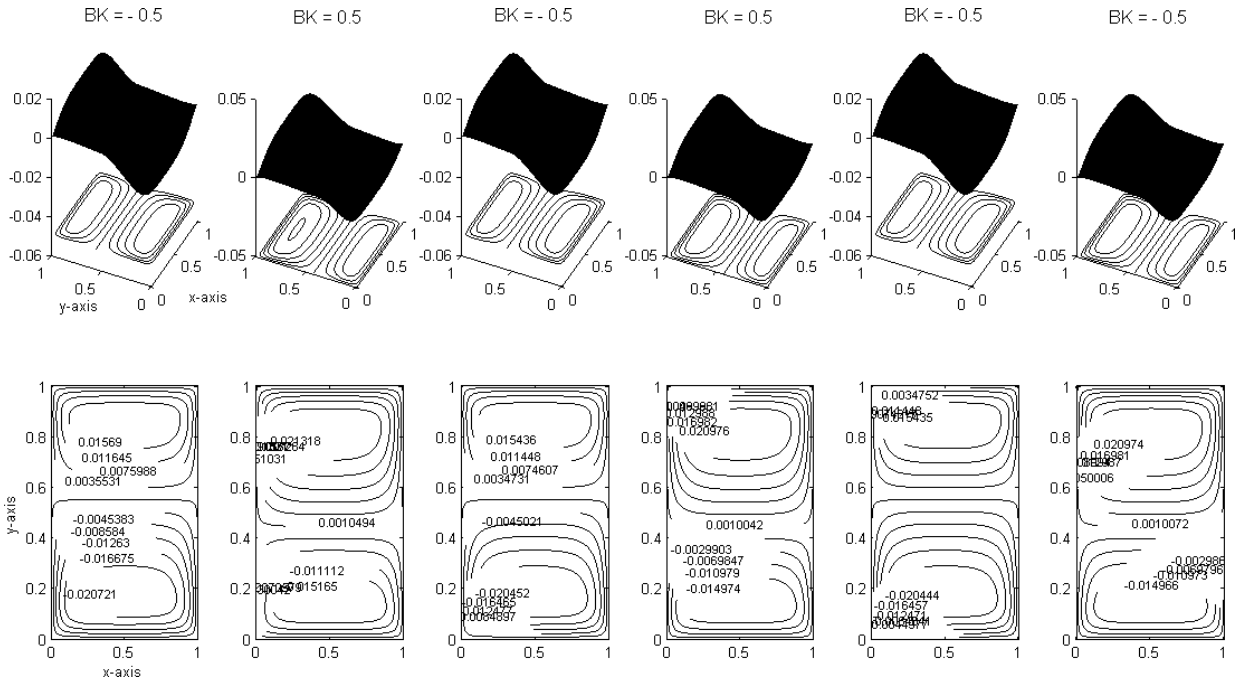

FIG. 2.

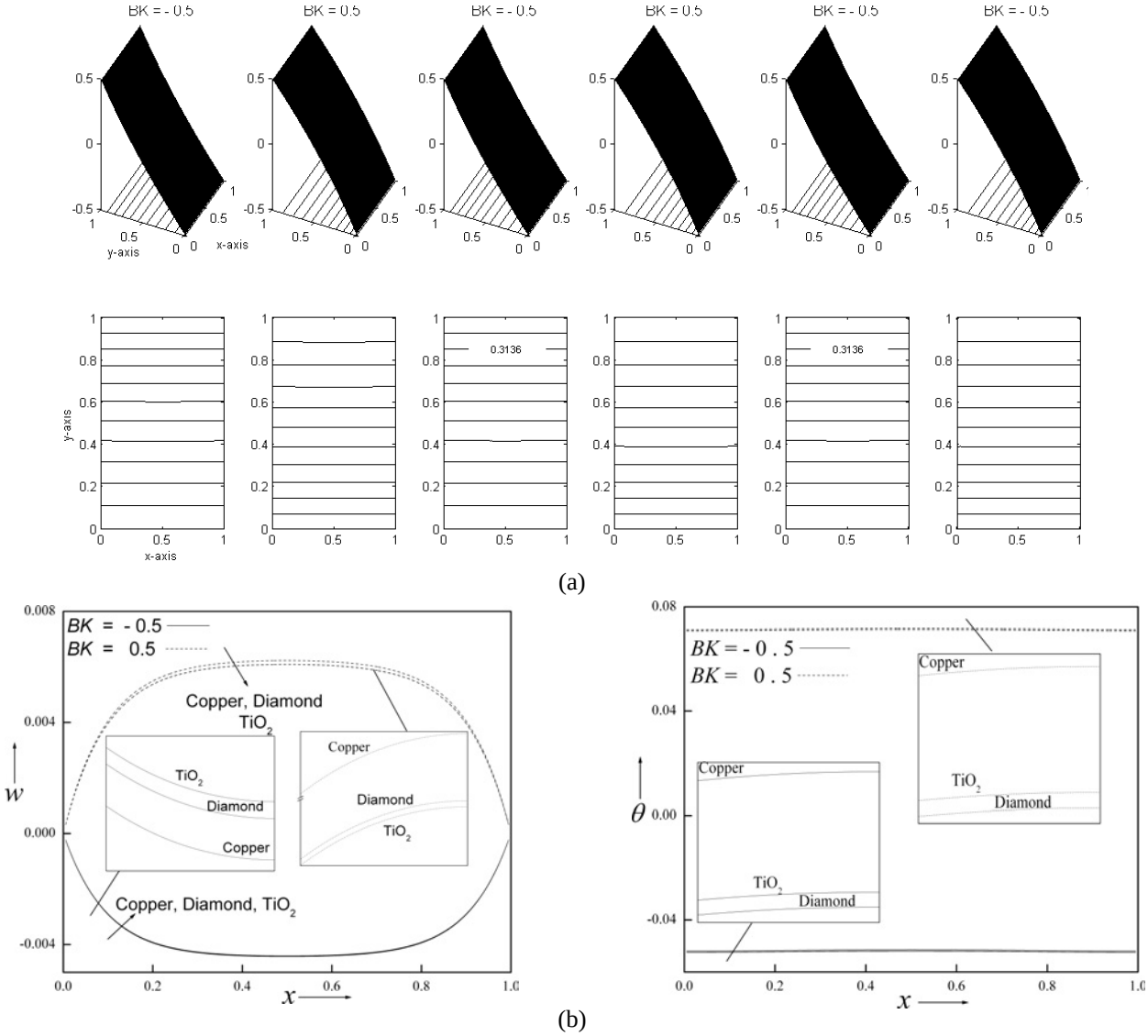

FIG. 2: (a) Velocity and temperature contours for different nanofluids and BK values with Gr = 10, Br = 1.0, Da = 0.01, I = 2.0, A = 1.0, and ϕ = 0.02; (b) velocity and temperature profiles for different nanofluids and BK values with Gr = 10, Br = 1.0, Da = 0.01, I = 2.0, A = 1.0, and ϕ = 0.02 at y = 0.1

contours are dense for values of $y < 0.5$ and $BK < 0$ and dense for values of $y > 0.5$ and $BK > 0$ for all of the nanoparticles under study, indicating that the flow moves in the upward direction of the duct as the thermal conductivity parameter BK increases. However, the contours of the temperature do not indicate any significant variations for the effects of BK on all of the nanoparticles. Thus, if one views carefully the three-dimensional picture, it can be seen that the curvature of the temperature field is convex for $BK < 0$ and concave for $BK > 0$ for all of the nanoparticles. Figure 2(b) better illustrates the effect of BK on different nanofluids. The flow values are negative for $BK < 0$ and positive for $BK > 0$. Titanium oxide is operative (maximum) for $BK < 0$ and copper is operative for $BK > 0$ on the velocity, whereas copper is operative in the temperature field for all values of BK when compared with the other nanoparticles.

Figures 3–9 present graphs of the results obtained using water as the base fluid and copper as the nanoparticle. Figures 3(a) and 3(b) illustrate the influence of thermal conductivity parameter BK on the flow field. It is very

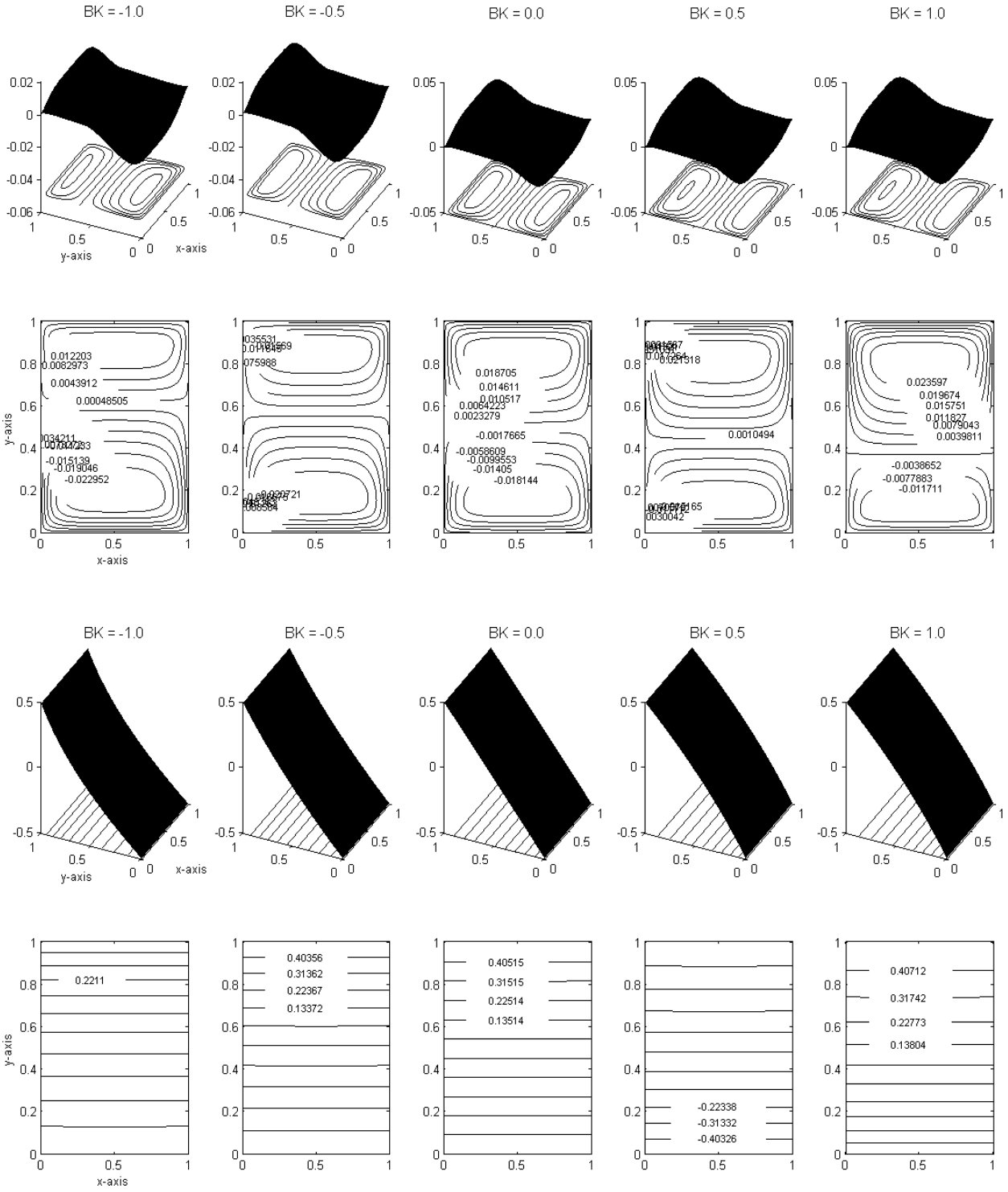

(a)

FIG. 3.

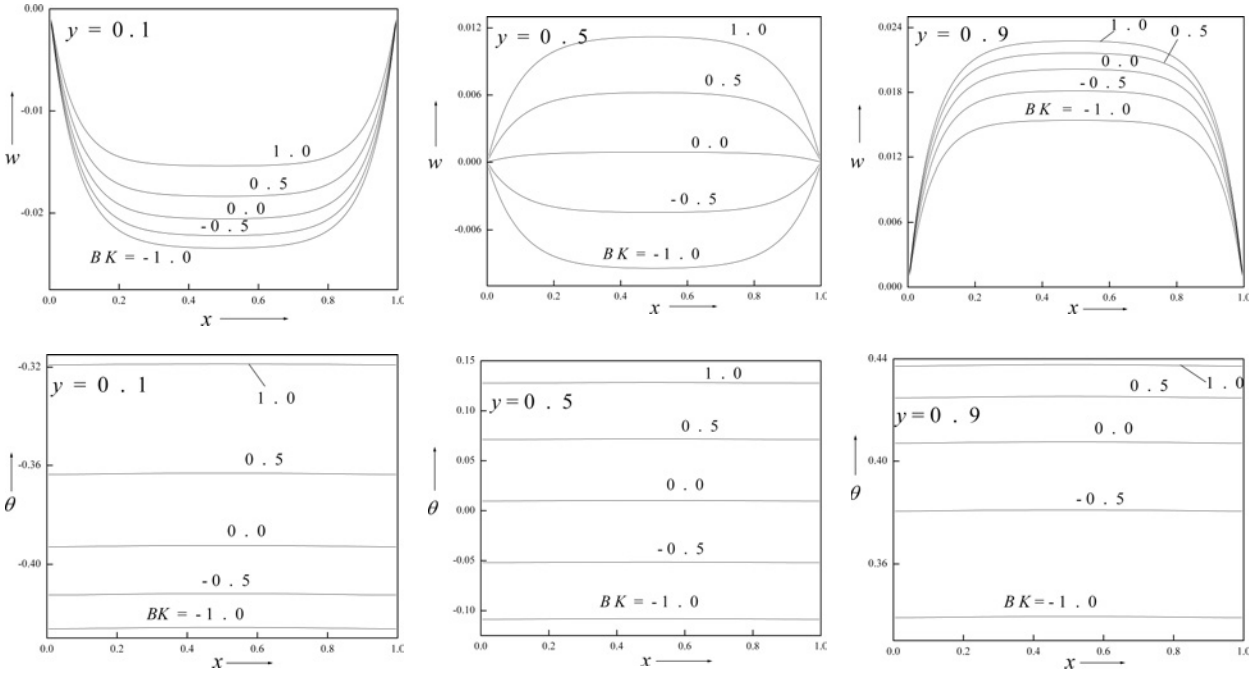

(b)

FIG. 3: (a) Velocity and temperature contours for different values of BK with Gr = 10, Br = 1.0, Da = 0.01, I = 2.0, A = 1.0, and ϕ = 0.02 for copper nanoparticles; (b) velocity and temperature profiles for different values of BK with Gr = 10, Br = 1.0, Da = 0.01, I = 2.0, A = 1.0, and ϕ = 0.02 at y = 0.1, 0.5, and 0.9 for copper nanoparticles

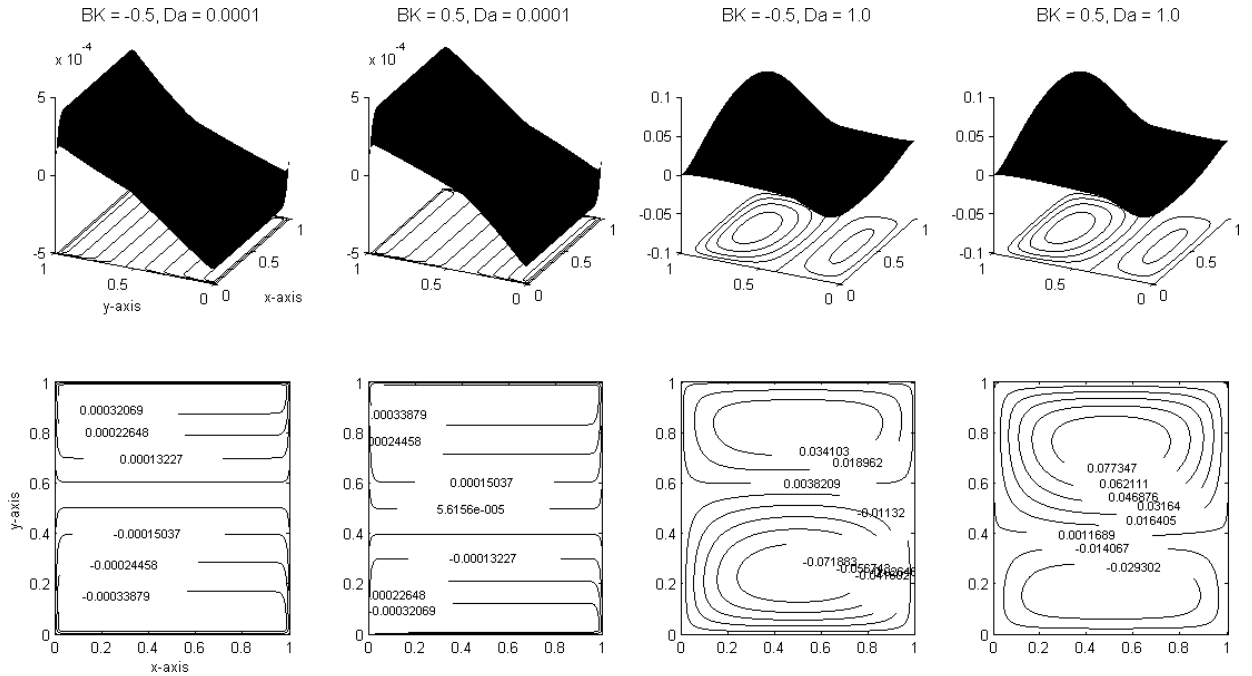

(a)

FIG. 4.

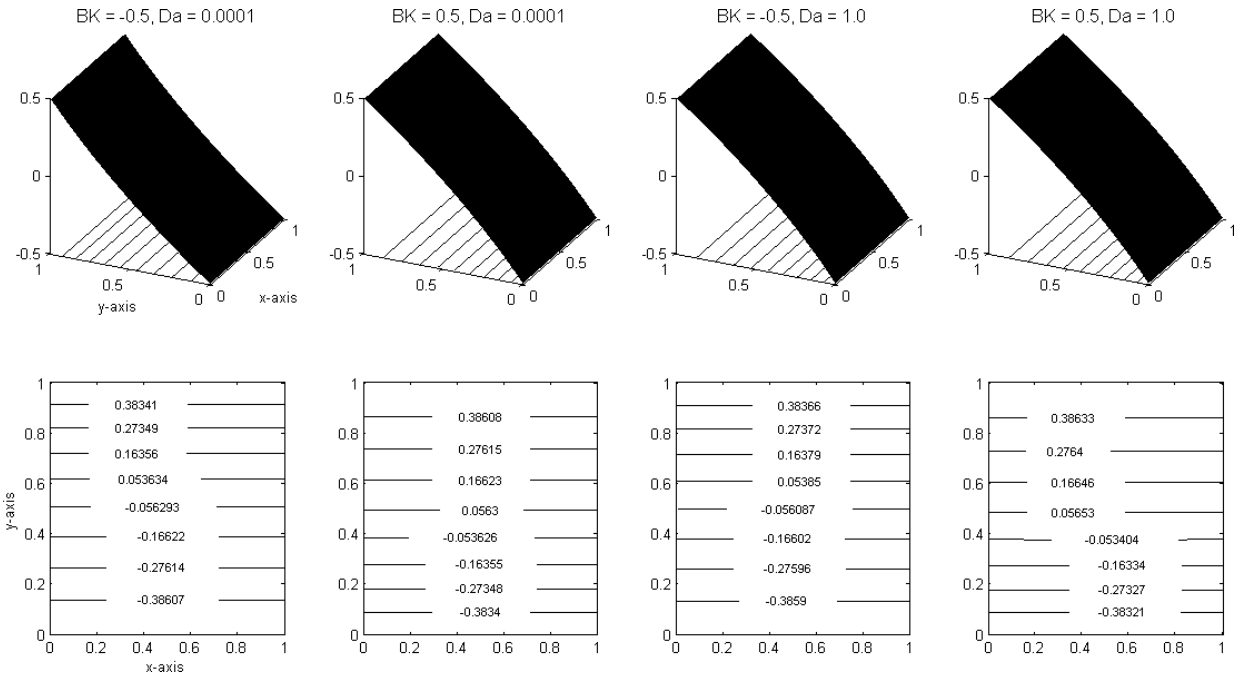

(b)

FIG. 4: Velocity and temperature contours (a) and velocity and temperature profiles (b) for different values of BK and Da with Gr = 10, Br = 1.0, I = 2.0, A = 1.0, and ϕ = 0.02 for copper nanoparticles

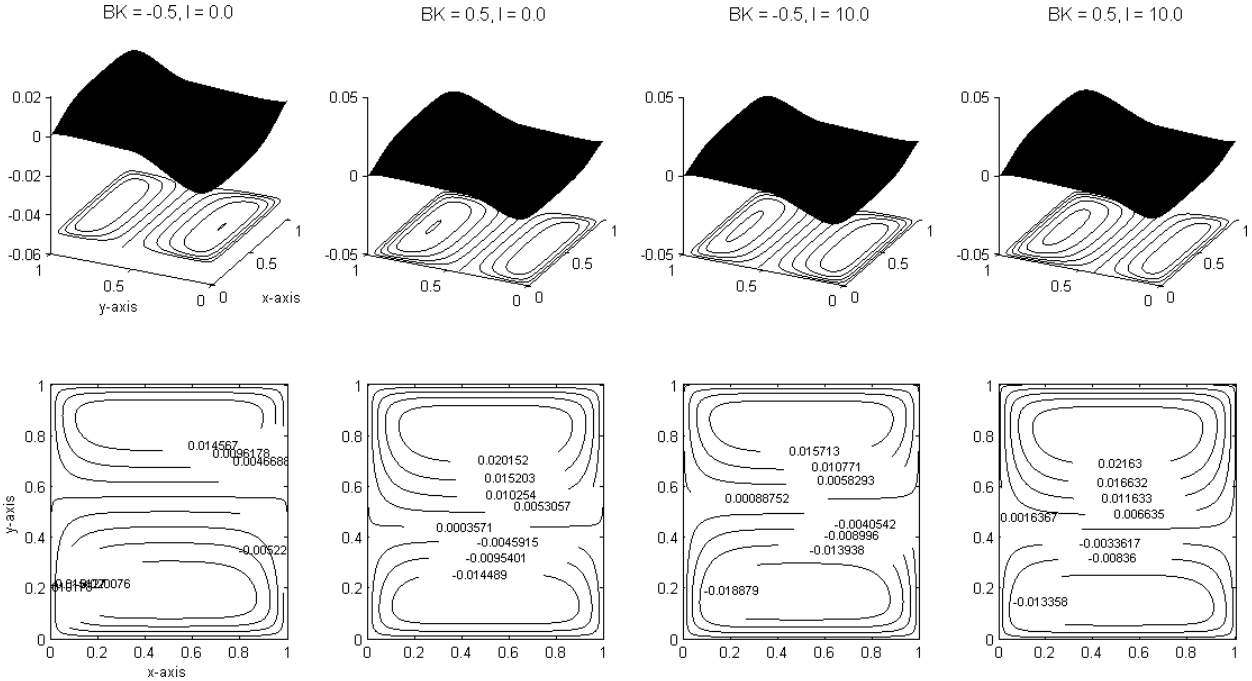

FIG. 5.

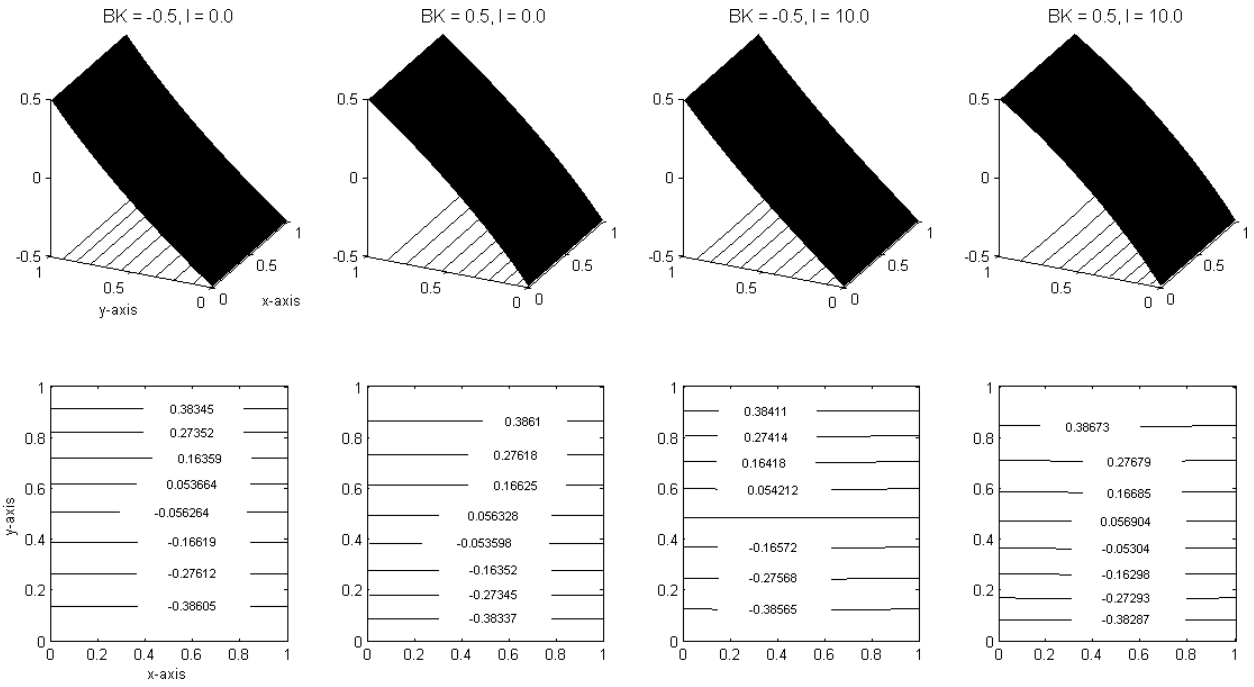

(a)

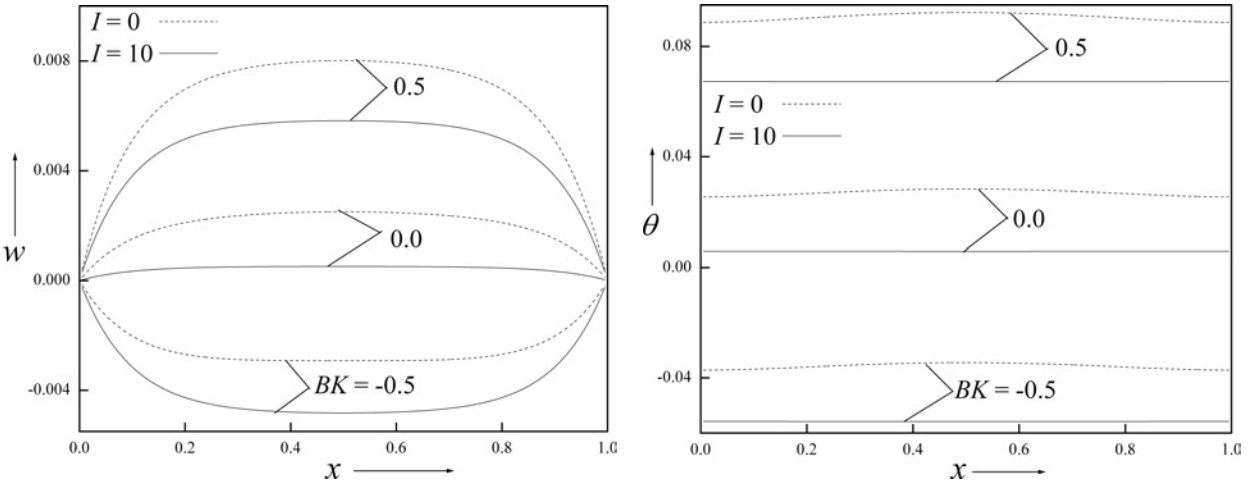

(b)

FIG. 5: Velocity and temperature contours (a) and velocity and temperature profiles (b) for different values of *BK* and *I* with Gr = 10, Br = 1.0, Da = 0.01, *A* = 1.0, and ϕ = 0.02 for copper nanoparticles

clear from the velocity contours in Fig. 3(a) that the velocity moves in the upward direction along the y-axis as BK increases. For constant thermal conductivity $(BK = 0)$, the total number of contours are equal in both the downward and upward regions from the midsection of $y(y = 0)$. The temperature contours do not vary much with the variation of BK. However, the three-dimensional graph displays the temperature field as being convex in nature for $BK < 0$, concave in nature for $BK > 0$, and linear for $BK = 0$. In order to know the effect of BK at different positions of

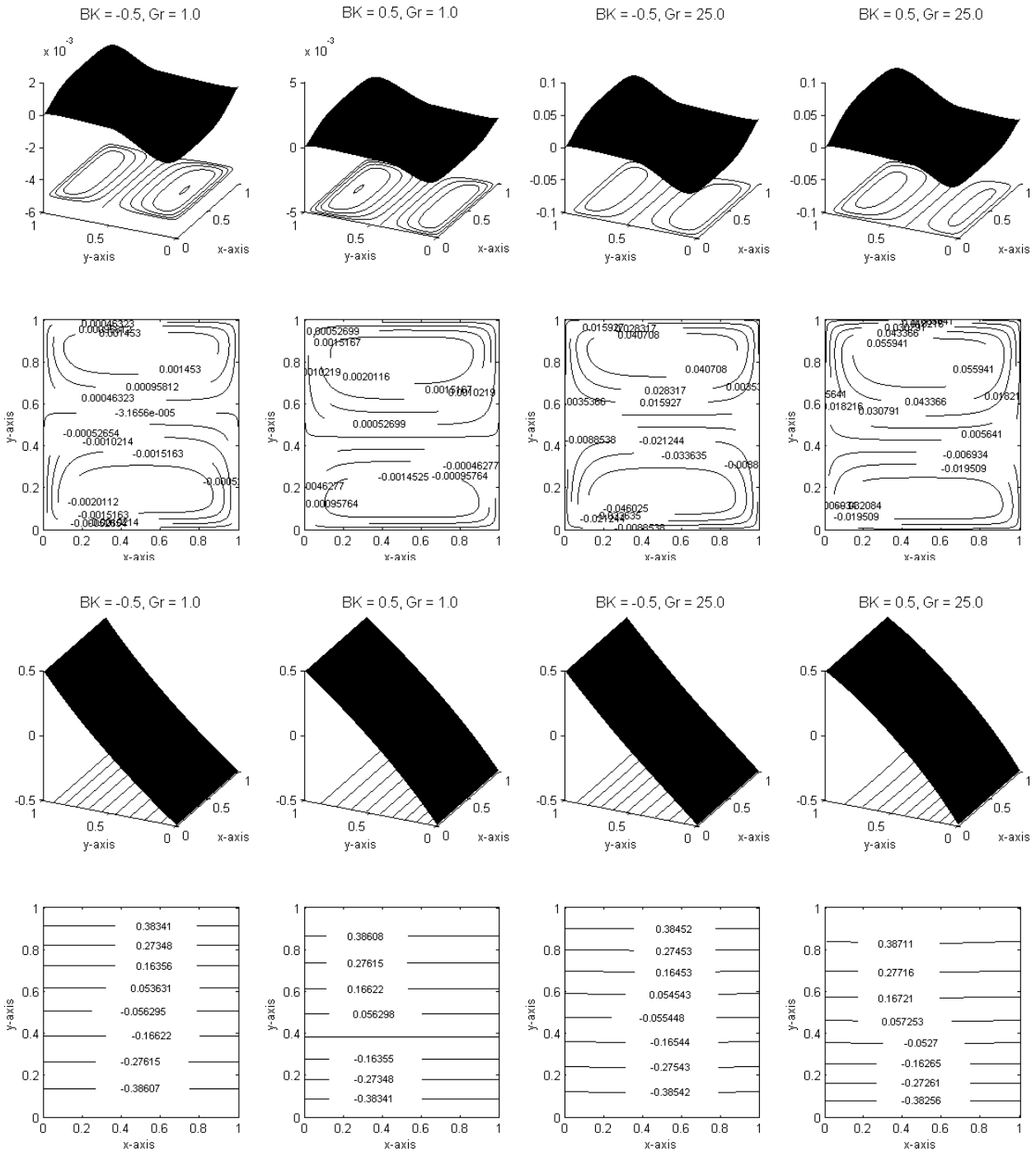

(a)

FIG. 6.

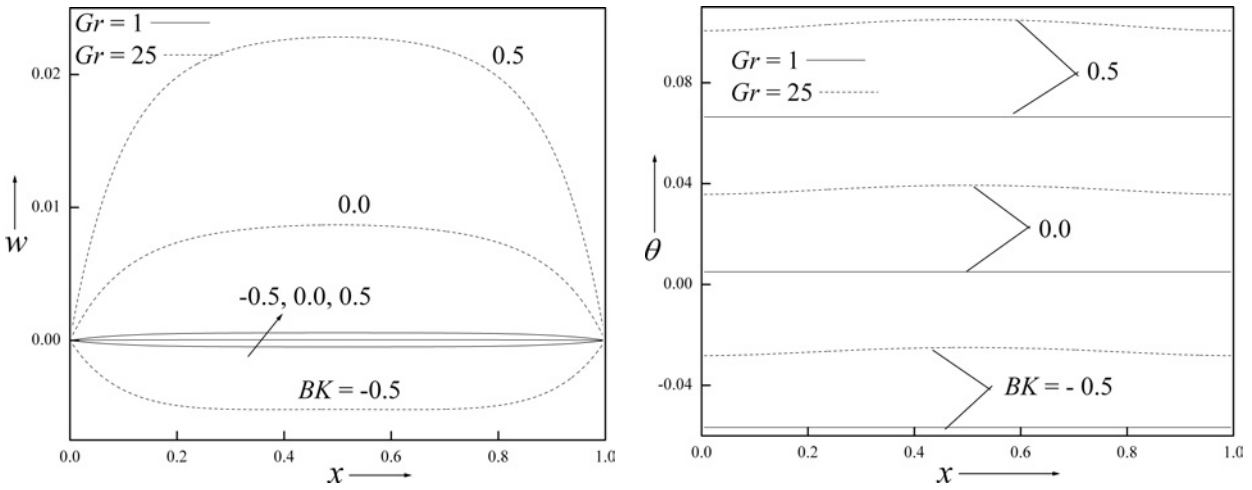

(b)

FIG. 6: Velocity and temperature contours (a) and velocity and temperature profiles (b) for different values of BK and Gr with Br = 1.0, Da = 0.01, I = 2.0, A = 1.0, and ϕ = 0.02 for copper nanoparticles

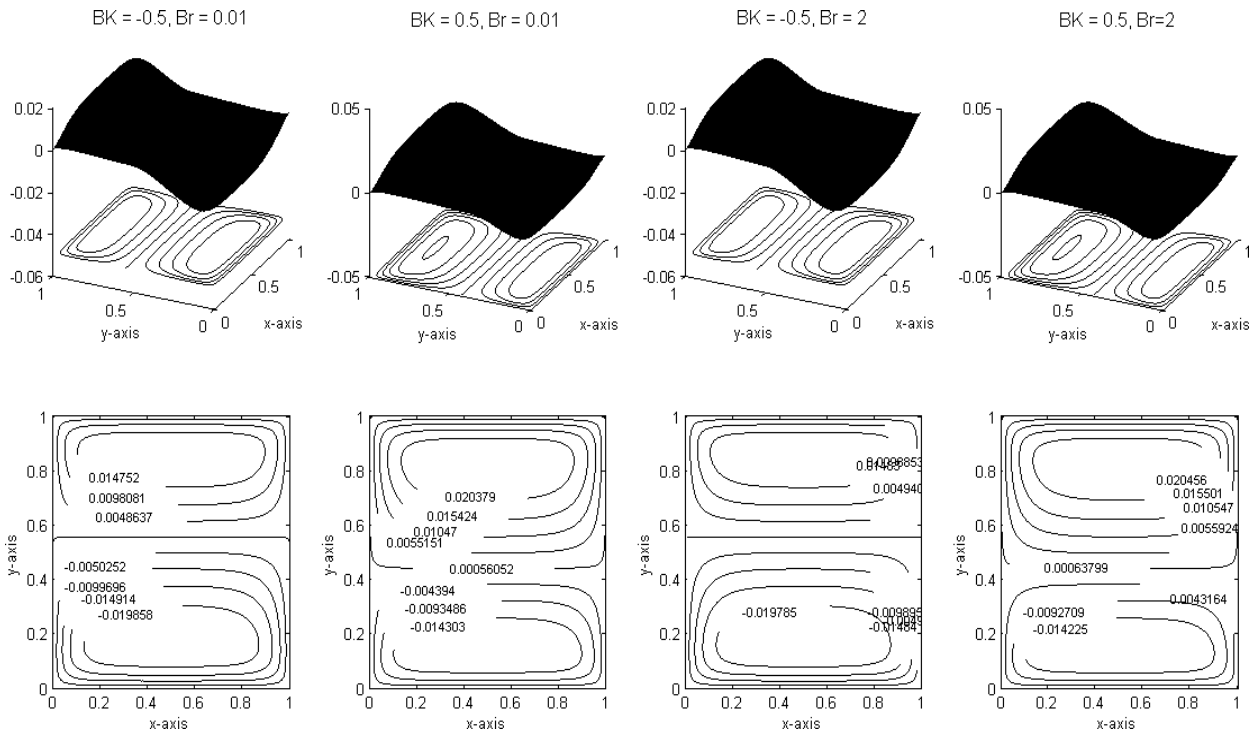

FIG. 7.

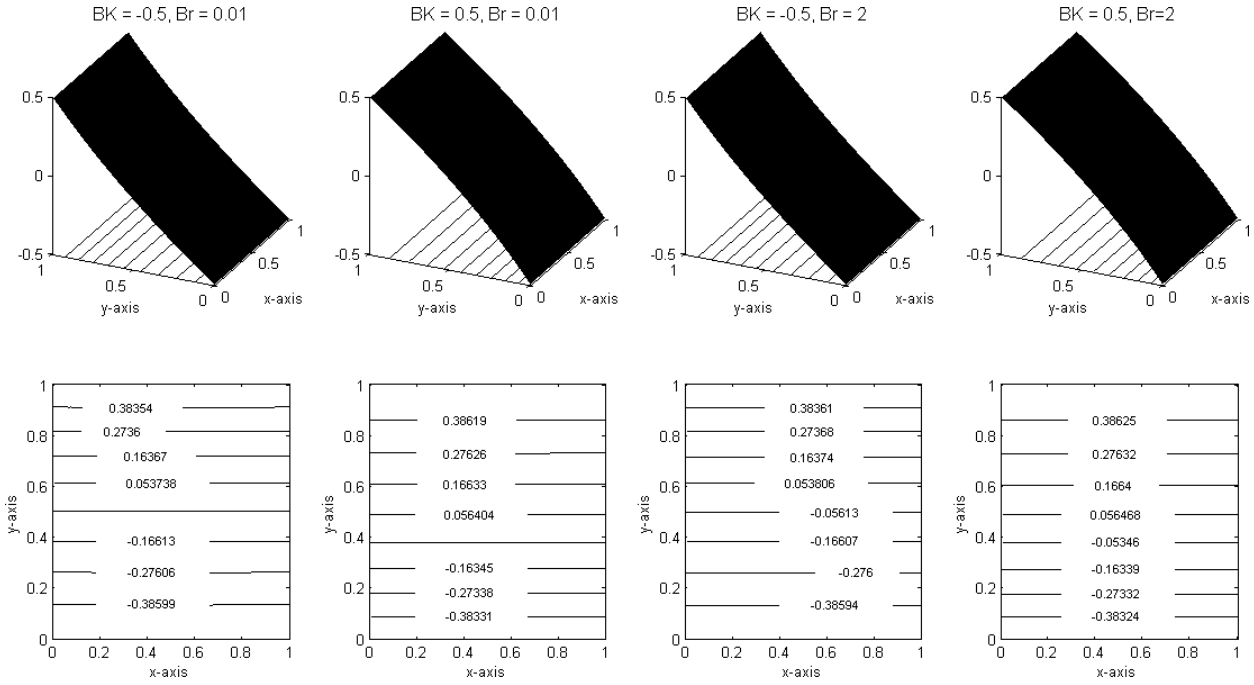

(a)

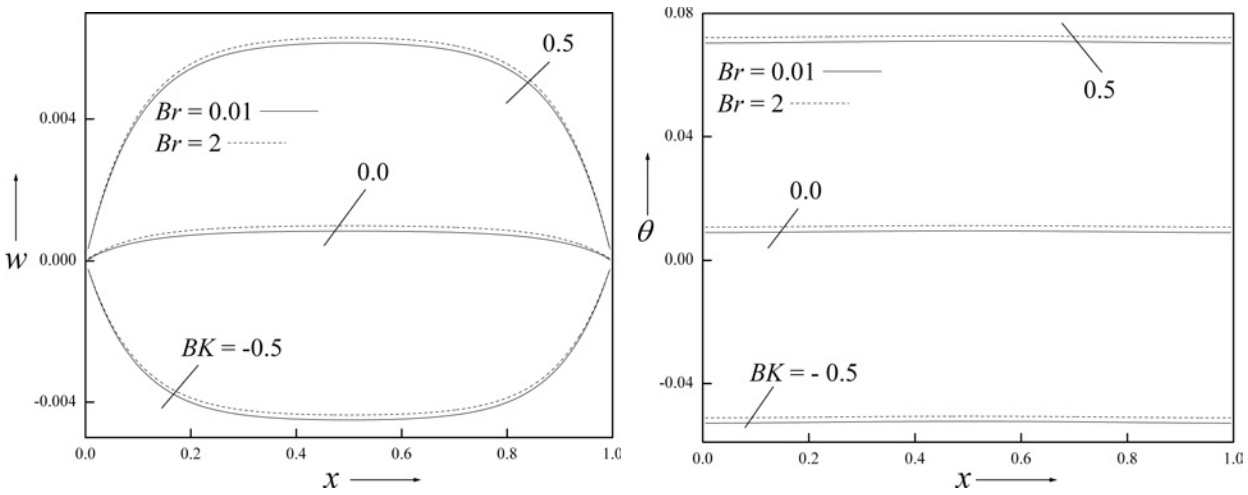

(b)

FIG. 7: Velocity and temperature contours (a) and velocity and temperature profiles (b) for different values of BK and Br with Gr = 10, Da = 0.01, I = 2.0, A = 1.0, and ϕ = 0.02 for copper nanoparticles

the duct, plots were drawn at $y = 0.1, 0.5$, and 0.9, as shown in Fig. 3(b). At any position of y, both the velocity and temperature increases as BK increases. The velocity profiles are in the downward direction at $y = 0.1$, symmetric at $y = 0.0$, and in the upward direction at $y = 0.9$, whereas the temperature profiles are similar at any position of y.

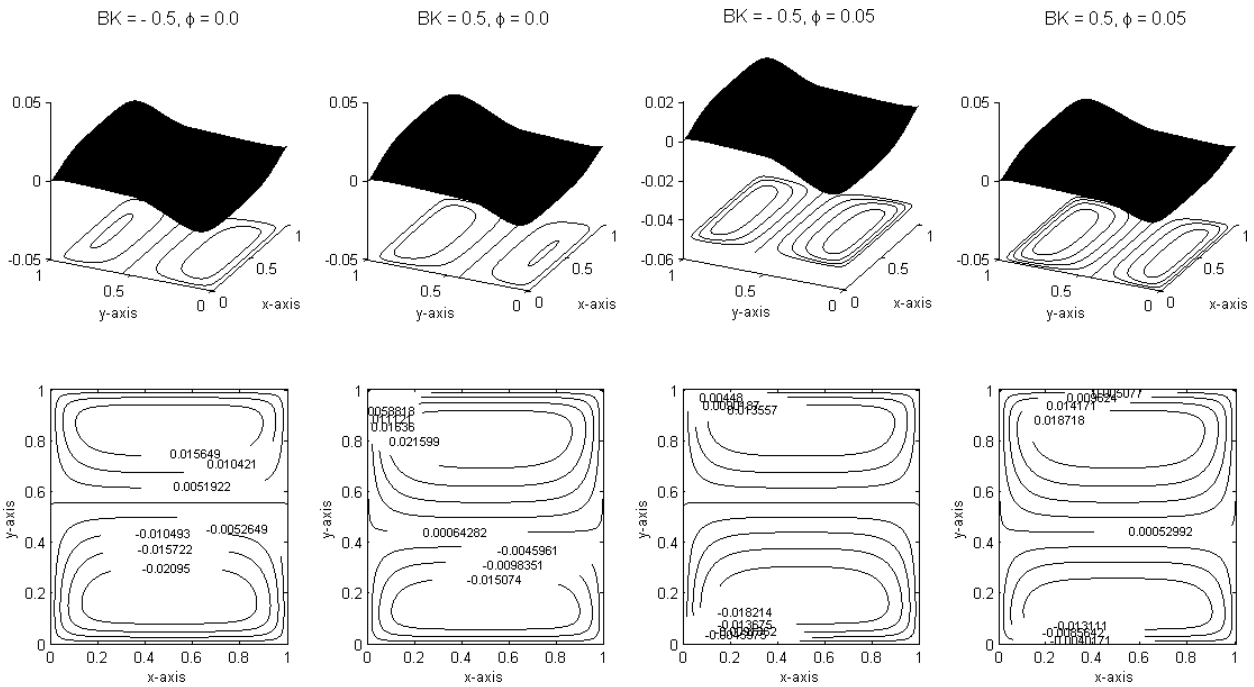

(a)

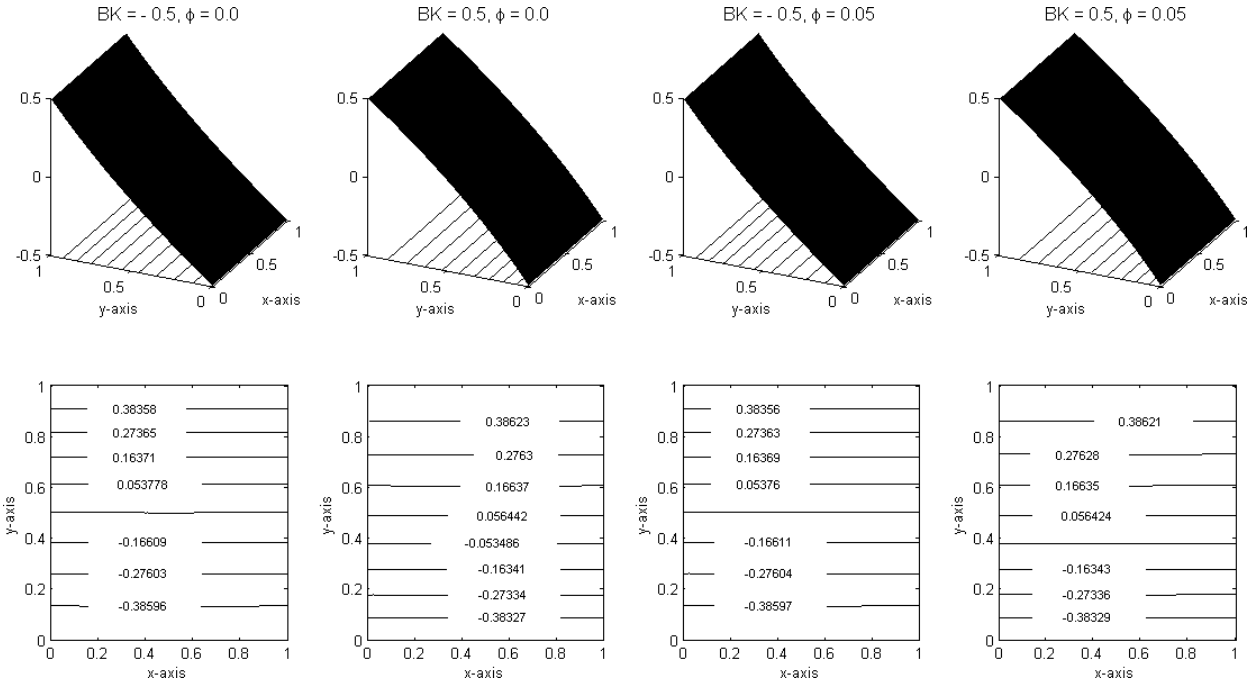

(b)

FIG. 8: Velocity and temperature contours (a) and velocity and temperature profiles (b) for different values of BK and ϕ with Gr = 10, Br = 1.0, Da = 0.01, I = 2.0, and A = 1.0 for copper nanoparticles

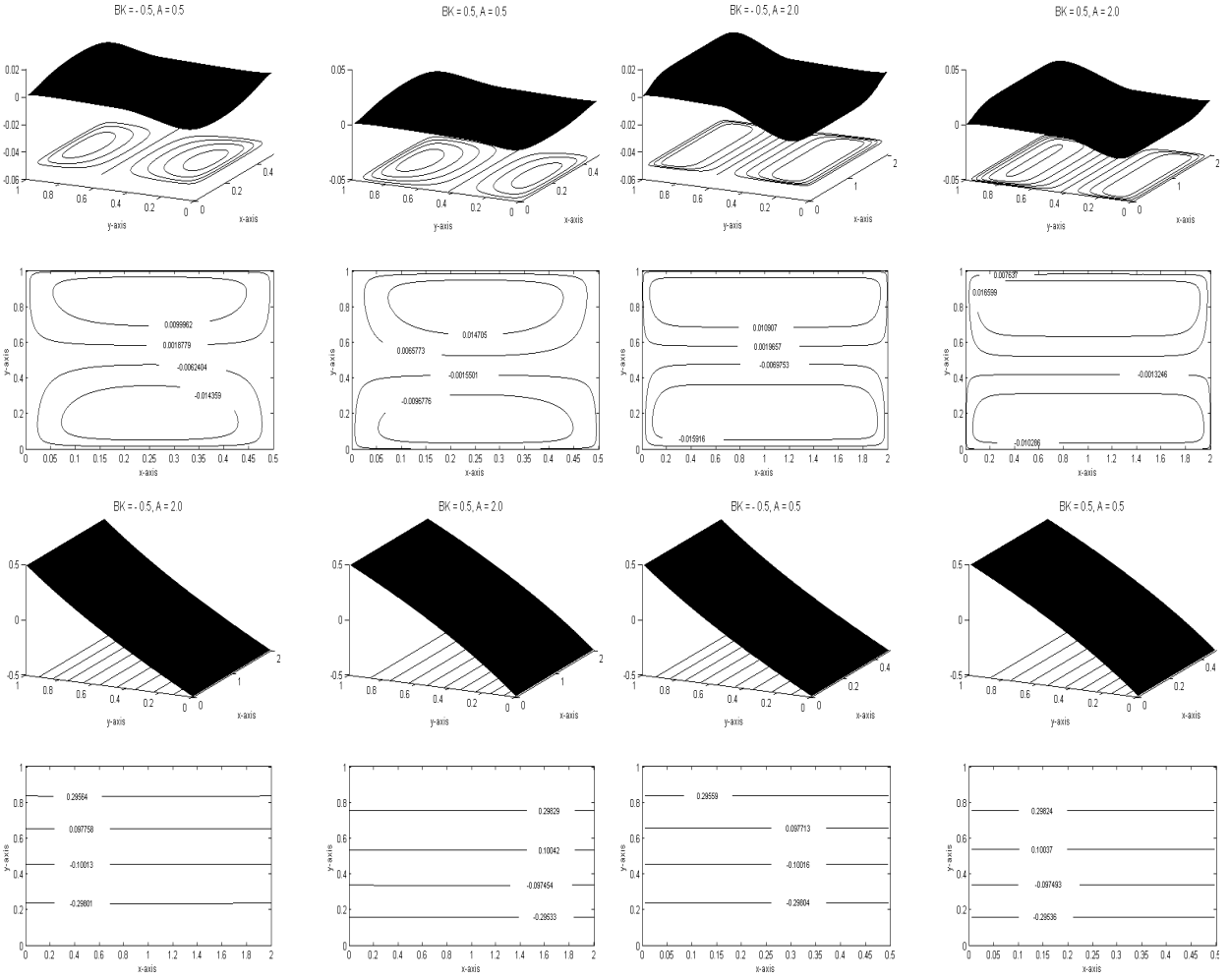

(a)

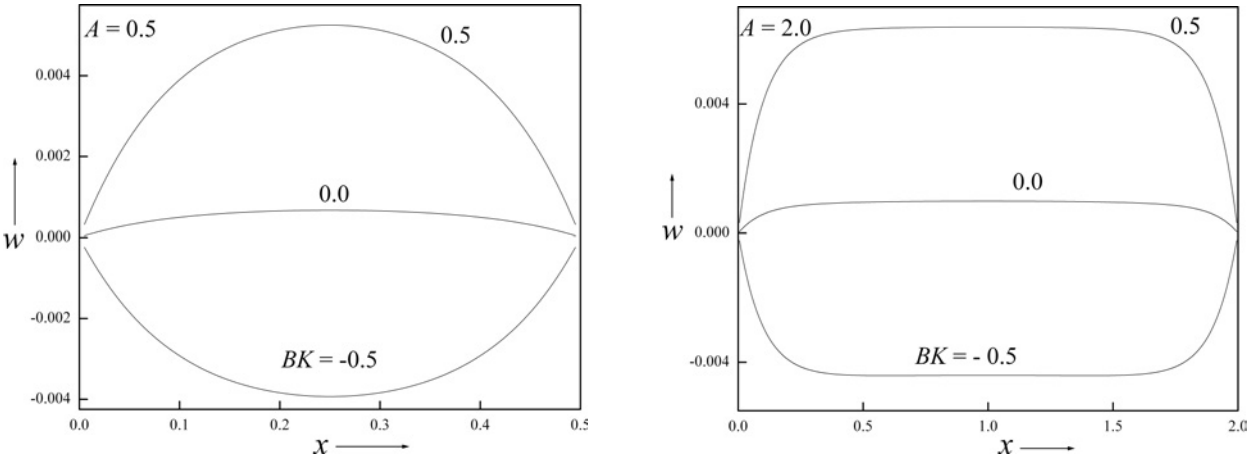

FIG. 9.

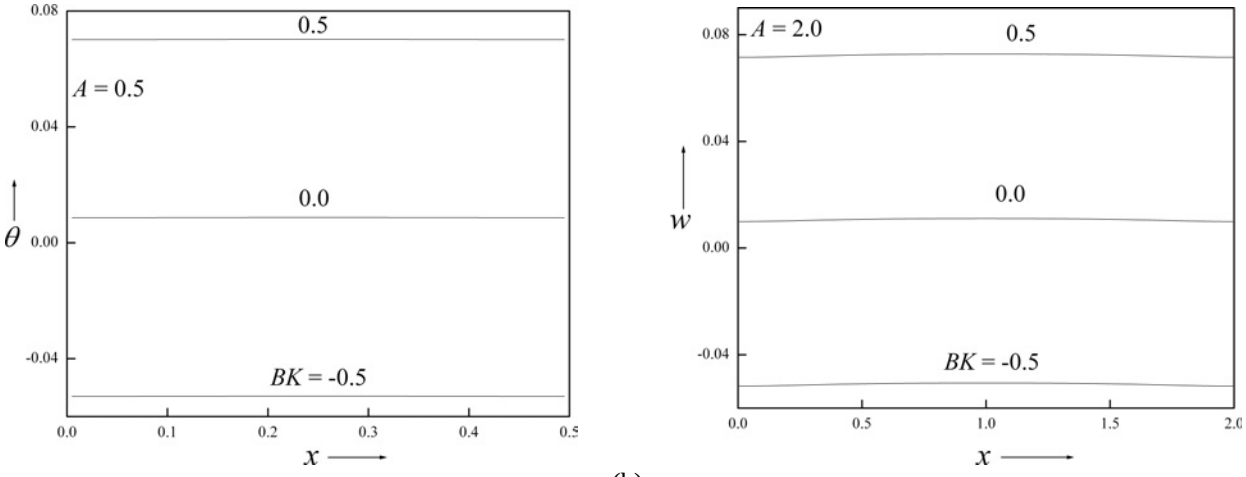

(b)

FIG. 9: Velocity and temperature contours (a) and velocity and temperature profiles (b) for different values of BK and A with Gr = 10, Br = 1.0, Da = 0.01, I = 2.0, and ϕ = 0.02 for copper nanoparticles

Figures 4(a) and 4(b) present the contours and profiles for variations of the Darcy number Da and variable thermal conductivity parameter BK. Small values of Da indicate flat contours, whereas large values of Da indicate the contours have become circular. The curvatures of the velocity contours in three dimensions show clear distinctions for the effects of Da on the flow. As Da increases, the flow increases in the upward direction for any value of BK. Once again, the temperature field is not significantly affected by the variations of both Da and BK, as seen in Fig. 4(a). The effects of Da and BK on the flow are visible in Fig. 4(b) when the profiles are drawn fixing y and varying x. As the Darcy number increases, the flow increases in the downward direction for $BK < 0$ and in the upward direction for $BK > 0$, and the profiles for the constant thermal conductivity $(BK = 0)$ parameter lie below $BK > 0$ and above $BK < 0$. The effect of Da on the flow is obvious because the lower values of the Darcy number corresponds to the densely packed porous medium, and hence the flow is reduced. The effect of inertial parameter I is depicted in Figs. 5(a) and 5(b). Figure 5(a) shows that the velocity or temperature fields are not significantly affected by the absence $(I = 0)$ or presence $(I = 10)$ of the inertial parameter. The effect of BK is visible, which remains the same as illustrated in Fig. 3(a). The effect of inertial parameter I is observed in the one-dimensional graph in Fig. 5(b), which clearly indicates that as I increases both the velocity and temperature decreases for all values of BK. The reduction in the flow is due to the inertial effect.

The effects of Grashof number Gr and Brinkman number Br are depicted in Figs. 6 and 7, respectively, in a square duct for variations of BK. One can conclude from Figs. 6(a) and 7(a) that as Gr and Br increases the flow is enhanced in the upward direction for both negative and positive values of BK. One can view from the two-dimensional graphs that the number of contours increase in the region $0.5 \leq y \leq 1.0$ as Gr and Br increases. The three- and two-dimensional graphs do not explicitly indicate the effects of Gr and Br on the temperature field. However, the curvature of the temperature is convex for $BK < 0$, concave for $BK > 0$, and linear for $BK = 0$. Thus, from the one-dimensional graphs [Figs. 6(b) and 7(b)] one can easily predict that as Gr and Br increase the flow field is enhanced. The effects of BK for variations of Gr and Br show a similar nature, as presented in Fig. 3. That is, the flow increases in the downward direction with an increase in the negative values of BK and increases in the upward direction with an increase in the positive values of BK. The enhancement in the flow for increasing values of the Grashof number occurs because as Gr increases the buoyancy force also increases. The increase in Br increases the viscous dissipation effect, which in turn increases the buoyancy force and hence the flow is enhanced.

Figure 8(a) shows contour maps of the velocity and temperature for Cu-water nanofluids in a square cavity at different values of nanoparticle volume fraction ϕ. The effect of ϕ on the flow is not significant, as shown in Fig. 8(a). However, Fig. 8(b) indicates that as ϕ increases, the velocity and temperature values decreases for $BK > 0$ and

increase for $BK < 0$, while little variation is observed for $BK = 0$. High values of ϕ cause the fluid to become more viscous, which causes the movement of the fluid in the cavity to slow down, resulting in a reduced convection effect. The effects of BK are predominant on the flow. As BK increases the flow increases in the upward direction for both regular and nanofluids. The effect of considering different shapes of the duct can be seen by changing of values of the aspect ratio A. For values of $A = 0.5$, the duct is narrow and for $A = 2$, the duct becomes wider. Figure 9(a) shows the flow contours for different values of A. The velocity contours are circular in nature for $A = 0.5$ and become rectangular for $A = 2.0$. The temperature contours do not show any changes for the effects of A. The effect of variable thermal conductivity parameter BK on the curvature of temperature is visible. It is convex for negative values of BK, concave for positive values of BK, and linear for $BK = 0$. Figure 9(b) also indicates that the profiles are narrow for small values of A and flatten as A increases. The temperature profiles look similar for variations of A and increase as BK increases for both values of A.

The effects of the physical properties such as volumetric flow rate Q, skin friction dw/dy at $y = 0$ and 1 and dw/dx at $x = 0$ and 1, and the rate of heat transfer on the pertinent parameters are tabulated in Tables 1, 2, and 3, respectively. It can be seen from Table 1 that as thermal conductivity parameter BK increases, the volumetric flow rate increases for all of the pertinent parameters and also for all of the nanoparticles under study. The volumetric flow rate decreases for increasing values of ϕ, and I, whereas it increases for increasing values of Da, Gr, Br, and A. The shear stress dw/dy at $y = 0$ decreases in magnitude as BK increases, whereas it increases at $y = 1$ for all of the governing parameters. The shear stress dw/dy at both plates increases with increasing values of ϕ, Da, Gr, Br, and A. The shear stress at $y = 0$ decreases and increases at $y = 1$ for increasing values of I.

Shear stress dw/dx at $x = 0$ increases and dw/dx at $x = 1$ decreases as BK increases for all of the governing parameters and also for all of the nanoparticles. At $BK = 0.5$, shear stress dw/dx increases in magnitude with increases in all of the governing parameters. At $BK = 0.5$, shear stress dw/dx at $x = 0$ and 1 increases in magnitude with increasing values of ϕ, Da, I, Gr, Br, and A, as seen in Table 2. The rate of heat transfer $d\theta/dy$ increases at $y = 0$ and decreases at $y = 1$ (Table 3) for all of the pertinent parameters at all the values of BK. However, the rate of heat transfer at $y = 0$ and 1 is higher for nanofluids when compared with regular fluid. The rate of heat transfer is optimal for silver nanoparticle when compared with the other nanoparticles. However, there is not much differences in the value of the rate of heat transfer for all of the nanoparticles.

5. CONCLUSIONS

The problem of steady natural convection heat transfer in a differentially heated enclosure filled with a nanofluid saturated with a porous medium was investigated in this study using a variable thermal conductivity model. The governing equations were solved numerically using the well-known finite-difference method of second-order accuracy. Various representative numerical results for a wide range of pertinent parameters were presented. The variable thermal conductivity parameter enhanced the flow in the upward direction for positive values and in the downward direction for negative values of the variable conductivity parameter for all values of the governing parameters. The velocity field was enhanced with increasing values of the Darcy, Grashof, and Brinkman numbers, and the aspect ratio, and a reverse effect was observed for the inertial and solid volume fraction. The temperature field was not significantly distorted with the variations of any of the governing parameters. However, the curvature of the temperature field was convex for negative values and concave for positive values of the variable thermal conductivity parameter. The rate of heat transfer was enhanced for the nanofluid when compared with the regular fluid for all of the nanoparticles. Not much variations was found in the rate of heat transfer by using different nanoparticles. The results obtained are in agreement with the results given in Umavathi (2015a) for the regular fluid. The results of the effect of the solid volume fraction and different nanoparticles in the absence of porous medium for constant properties agree with the results obtained by Umavathi and Sheremet (2016).

ACKNOWLEDGMENTS

J.C. Umavathi gratefully acknowledges the supervisor (Professor Maurizio Sasso) and coordinator (Professor Matteo Savino) for providing financial support under the ERUSMUS MUNDUS “Featured Europe and South/South-East Asia mobility Network FUSION” for Post-Doctoral Research.

TABLE 1: Values of the volumetric flow rate and skin friction for Gr = 10, Br = 1, Da = 0.01, I = 2.0, A = 1, and ϕ = 0.02

BK	Q	$(dw/dy)\|_{y=0}$	$(dw/dy)\|_{y=1}$	Q	$(dw/dy)\|_{y=0}$	$(dw/dy)\|_{y=1}$
	ϕ = 0			ϕ = 0.05		
–0.5	-2.763×10^{-3}	–0.184028	–0.169049	-2.424×10^{-3}	–0.206539	–0.189528
0.0	2.808×10^{-4}	–0.177064	–0.178751	2.174×10^{-4}	–0.198732	–0.200415
0.5	3.331×10^{-3}	–0.167290	–0.185692	2.865×10^{-3}	–0.187775	–0.208205
	Da = 0.0001			Da = 1		
–0.5	-3.858×10^{-5}	-2.269×10^{-2}	-2.242×10^{-2}	-1.368×10^{-2}	–0.366250	–0.288710
0.0	7.372×10^{-8}	-2.258×10^{-2}	-2.258×10^{-2}	1.860×10^{-3}	–0.325754	–0.336043
0.5	3.873×10^{-5}	-2.242×10^{-2}	-2.269×10^{-2}	1.756×10^{-2}	–0.277222	–0.376395
	I = 0.0			I = 10.0		
–0.5	-2.838×10^{-3}	–0.193265	–0.176096	-1.781×10^{-3}	–0.189988	–0.179914
0.0	4.148×10^{-5}	–0.185983	–0.186262	1.141×10^{-3}	–0.182606	–0.190146
0.5	2.919×10^{-3}	–0.175789	–0.193516	4.108×10^{-3}	–0.172116	–0.197555
	Gr = 1			Gr = 25		
–0.5	-2.876×10^{-4}	-1.933×10^{-2}	-1.759×10^{-2}	-3.246×10^{-3}	–0.471441	–0.454807
0.0	2.293×10^{-7}	-1.861×10^{-2}	-1.861×10^{-2}	4.210×10^{-3}	–0.452587	–0.480600
0.5	2.881×10^{-4}	2.067×10^{-3}	-2.067×10^{-3}	1.179×10^{-2}	–0.425689	–0.499319
	Br = 0.01			Br = 2		
–0.5	-2.661×10^{-3}	–0.192686	–0.176682	-2.581×10^{-3}	–0.192443	–0.176991
0.0	2.158×10^{-4}	–0.185417	–0.186846	2.986×10^{-4}	–0.185145	–0.187130
0.5	3.101×10^{-3}	–0.175209	–0.194123	3.183×10^{-3}	–0.174905	–0.194381
	A = 0.5			A = 2.0		
–0.5	-2.071×10^{-3}	–0.168568	–0.155995	-2.891×10^{-3}	–0.204620	–0.187345
0.0	1.460×10^{-4}	–0.162951	–0.163945	3.250×10^{-4}	–0.196485	–0.198618
0.5	2.366×10^{-3}	–0.154949	–0.169538	3.550×10^{-3}	–0.185126	–0.206737
	Cu			TiO_2		
–0.5	-2.621×10^{-3}	–0.192565	–0.176835	-2.606×10^{-3}	–0.189806	–0.174150
0.0	2.570×10^{-4}	–0.185281	–0.186987	2.294×10^{-4}	–0.182630	–0.184153
0.5	3.142×10^{-3}	–0.175058	–0.194251	3.071×10^{-3}	–0.172561	–0.191309
	Silver			Diamond		
–0.5	-2.623×10^{-3}	–0.193237	–0.177502	-2.610×10^{-3}	–0.189868	–0.174187
0.0	2.657×10^{-4}	–0.185927	–0.187690	2.265×10^{-4}	–0.182690	–0.184193
0.5	3.161×10^{-3}	–0.175665	–0.194981	3.069×10^{-3}	–0.172619	–0.191351

TABLE 2: Values of the skin friction for Gr = 10, Br = 1, Da = 0.01, I = 2.0, A = 1, and ϕ = 0.02

BK	$(dw/dx)\|_{x=0}$	$(dw/dx)\|_{x=1}$	$(dw/dx)\|_{x=0}$	$(dw/dx)\|_{x=1}$
	ϕ = 0		ϕ = 0.5	
–0.5	-1.803×10^{-2}	1.803×10^{-2}	-2.044×10^{-2}	2.044×10^{-2}
0.0	1.707×10^{-3}	-1.707×10^{-3}	1.699×10^{-3}	-1.699×10^{-3}
0.5	2.149×10^{-2}	-2.149×10^{-2}	2.388×10^{-2}	-2.388×10^{-2}
	Da = 0.0001		Da = 1.0	
–0.5	-1.944×10^{-3}	1.944×10^{-3}	-5.303×10^{-2}	5.303×10^{-2}
0.0	3.639E–6	–3.639E–6	7.356×10^{-3}	-7.356×10^{-3}
0.5	1.952×10^{-3}	-1.952×10^{-3}	6.853×10^{-2}	-6.853×10^{-2}
	I = 0.0		I = 10.0	
–0.5	-2.033×10^{-2}	2.033×10^{-2}	-1.348×10^{-2}	1.348×10^{-2}
0.0	3.268×10^{-4}	-3.268×10^{-4}	7.453×10^{-3}	-7.453×10^{-3}
0.5	2.097×10^{-2}	-2.097×10^{-2}	2.869×10^{-2}	-2.869×10^{-2}
	Gr = 1		Gr = 25	
–0.5	-2.063×10^{-3}	2.063×10^{-3}	-2.522×10^{-2}	2.522×10^{-2}
0.0	1.634×10^{-6}	-1.634×10^{-6}	2.810×10^{-2}	-2.810×10^{-2}
0.5	2.067×10^{-3}	-2.067×10^{-3}	8.235×10^{-2}	-8.235×10^{-2}
	Br = 0.01		Br = 2	
–0.5	-1.924×10^{-2}	1.924×10^{-2}	-1.861×10^{-2}	1.861×10^{-2}
0.0	1.399×10^{-3}	-1.399×10^{-3}	2.051×10^{-3}	-2.051×10^{-3}
0.5	2.210×10^{-2}	-2.210×10^{-2}	0.728034	0.407067
	A = 0.5		A = 2.0	
–0.5	-1.910×10^{-2}	1.910×10^{-2}	-1.885×10^{-2}	1.885×10^{-2}
0.0	1.333×10^{-3}	-1.333×10^{-3}	1.802×10^{-3}	-1.802×10^{-3}
0.5	2.179×10^{-2}	-2.179×10^{-2}	2.251×10^{-2}	-2.251×10^{-2}
	Cu		TiO_2	
-0.5	-1.892×10^{-2}	1.892×10^{-2}	-1.880×10^{-2}	1.880×10^{-2}
0.0	1.723×10^{-3}	-1.723×10^{-3}	1.543×10^{-3}	-1.543×10^{-3}
0.5	2.242×10^{-2}	-2.242×10^{-2}	2.193×10^{-2}	-2.193×10^{-2}
	Silver		Diamond	
–0.5	-1.894×10^{-2}	1.894×10^{-2}	-1.882×10^{-2}	1.882×10^{-2}
0.0	1.780×10^{-3}	-1.780×10^{-3}	1.524×10^{-3}	-1.524×10^{-3}
0.5	2.255×10^{-2}	-2.255×10^{-2}	2.191×10^{-2}	-2.191×10^{-2}

TABLE 3: Values of rate of heat transfer for Gr = 10, Br = 1, Da = 0.01, I = 2.0, A = 1, and ϕ = 0.02

BK	$(dw/dy)\|_{y=0}$	$(dw/dy)\|_{y=1}$	$(dw/dy)\|_{y=0}$	$(dw/dy)\|_{y=1}$
	ϕ = 0		ϕ = 0.5	
–0.5	0.413235	0.650020	0.476442	0.754678
0.0	0.514212	0.485341	0.593023	0.563700
0.5	0.683052	0.386199	0.787924	0.448741
	Da = 0.00001		Da = 1.0	
–0.5	0.424750	0.706861	0.447161	0.682072
0.0	0.530863	0.530074	0.552679	0.506993
0.5	0.707707	0.423994	0.731927	0.399875
	I = 0.0		I = 10.0	
–0.5	0.427516	0.703152	0.476179	0.637040
0.0	0.534010	0.526915	0.586405	0.465996
0.5	0.711403	0.421217	0.773661	0.361221
	G = 1		G = 25	
–0.5	0.424538	0.707163	0.501747	0.594527
0.0	0.530615	0.530322	0.615917	0.426730
0.5	0.707405	0.424206	0.810689	0.323450
	Br = 0.01		Br = 2	
–0.5	0.434888	0.694591	0.440950	0.686162
0.0	0.541497	0.519129	0.548420	0.511917
0.5	0.719837	0.413444	0.728034	0.407067
	A = 0.5		A = 2.0	
–0.5	0.434594	0.694492	0.439593	0.688312
0.0	0.541471	0.519228	0.546712	0.513655
0.5	0.719934	0.413860	0.725952	0.408426
	Cu		TiO_2	
–0.5	0.437909	0.690405	0.433245	0.686318
0.0	0.544947	0.515548	0.538098	0.511522
0.5	0.723920	0.410278	0.713461	0.406392
	Silver		Diamond	
–0.5	0.438290	0.689940	0.436649	0.692148
0.0	0.545355	0.515132	0.543638	0.517116
0.5	0.724397	0.409878	0.722452	0.411788

REFERENCES

Anyakoha, M.W., *New School Physics*, 3rd ed., Onitsha, Nigeria: Africana First Publisher Plc., 2010.

Astaninal, M.S., Sheremet, M.A., and Umavathi, J.C., Unsteady Natural Convection with Themperature-Dependent Viscosity in a Square Cavity Filled with a Porous Medium, *Transp. Porous Media*, vol. **110**, pp. 113–126, 2015.

Batchelor, G.K., *An Introduction to Fluid Dynamics*, London: Cambridge University Press, 1987.

Brinkman, H.C., The Viscosity of Concentrated Suspensions and Solution, *J. Chem. Phys*., vol. **20**, pp. 571–581, 1952.

Choi, S.U.S., Enhancing Thermal Conductivity of Fluids with Nanoparticles, *ASME Fluids Eng. Div.*, vol. **231**, pp. 99–105, 1995.

Choi, S.U.S., Zhang, Z.G., Yu, W., Lockwood, F.E., and Grulke, E.A., Anomalous Thermal Conductivity Enhancement in Nanotube Suspensions, *Appl. Phys. Lett.*, vol. **79**, pp. 2252–2254, 2001.

Darcy, H.P.G., *Les Fontaines Publiques de la Ville de Dijon*, Paris: Victor Dalmont, 1856.

Eastman, J.A., Choi, S.U.S., Li, S., Yu, W., and Thompson, L.J., Anomalously Increased Effective Thermal Conductivities of Ethylene Glycol-Based Nanofluids Containing Copper Nanoparticles, *Appl. Phys. Lett.*, vol. **78**, pp. 718–720, 2001.

Forchheimer, P., Wasserbewegung Durch Boden, *Z. Ver. Dtsch. Ing.*, vol. **45**, pp. 1782–1788, 1901.

Harms, T.M., Jog, M.A., and Manglik, R.M., Effects of Temperature-Dependent Viscosity Variations and Boundary Conditions on Fully Developed Laminar Steady Forced Convection in a Semicircular Duct, *J. ASME J. Heat Transf.*, vol. **120**, pp. 600–605, 1998.

Hashemi Amrei, S.M.H. and Dehkordi, A.M., Modeling and CFD Simulation of a Mixed-Convection Flow of Regular Fluids and Nanofluids in Vertical Porous and Regular Channels, *Heat Transf. Asian Res.*, vol. **43**, pp. 243–269, 2014.

Holditch, S.A. and Morse, R.A., The Effects of Non-Darcy Flow on the Behavior of Hydraulically Fractured Gas Wells, *J. Petrol. Technol.*, vol. **28**, pp. 1196–1179, 1976.

Kays, W.M. and Crawford, M.E., *Convective Heat and Mass Transf.*, New York: McGraw-Hill, 1993.

Lee, S., Choi, S.U.S., Li, S., and Eastman, J.A., Measuring Thermal Conductivity of Fluids Containing Oxide Nanoparticles, *ASME J. Heat Transf.*, vol. **121**, pp. 280–289, 1999.

Ling, J.X. and Dybbs, A., The Effect of Variable Viscosity on Forced Convection over a Flat Plate Submerged in a Porous Medium, *J. ASME J. Heat Transf.*, vol. **114**, pp. 1063–1065, 1992.

Maxwell, J., *A Treatise on Electricity and Magnetism*, 2nd ed., Cambridge, U.K.: Oxford University Press, 1904.

Meyers, T.G., Charpin, J.P.F., and Tshela, M.S., The Flow of a Variable Viscosity Fluid between Parallel Plates with Shear Heating, *Appl. Math. Modell.*, vol. **30**, pp. 799–815, 2006.

Mittal, N., Manoj, V., Kumar, D., and Satheesh, A., Numerical Simulation of Mixed Convection in a Porous Medium Filled with Water/Al_2O_3 Nanofluids, *Heat Transf. Asian Res.*, vol. **42**, pp. 46–59, 2013.

Nield, D.A. and Kuznetsov, A.V., Thermal Instability in a Porous Medium Layer Saturated by a Nanofluid, *Int. J. Heat Mass Transf.*, vol. **52**, nos. 25-26, pp. 5796–5801, 2009.

Pak, B.C. and Cho, Y.I., Hydrodynamic and Heat Transfer Study of Dispersed Fluids with Submicron Metallic Oxide Particles, *Exp. Heat Transf.*, vol. **11**, pp. 151–170, 1998.

Umavathi, J.C., Analysis of Flow and Heat Transfer in a Vertical Rectangular Duct Using a Non-Darcy Model, *Transp. Porous Media*, vol. **96**, pp. 527–545, 2013a.

Umavathi, J.C., Effect of Thermal Modulation on the Onset of Convection in a Porous Medium Layer Saturated by a Nanofluid, *Transp. Porous Media*, vol. **98**, pp. 59–79, 2013b.

Umavathi, J.C., Free Convective Flow in a Vertical Rectangular Duct Filled with Porous Matrix for Viscosity and Conductivity Variable Properties, *Int. J. Heat Mass Transf.*, vol. **81**, pp. 383–403, 2015a.

Umavathi, J.C., Rayleigh–Benard Convection Subject to Time Dependent Wall Temperature in a Porous Medium Layer Saturated by a Nanofluid, *Meccanica*, vol. **50**, pp. 981–994, 2015b.

Umavathi, J.C., Kumar J.P., and Sultana, J., Mixed Convection Flow in a Vertical Porous Channel with Boundary Conditions of the Third Kind with Heat Source/Sink, *J. Porous Media*, vol. **15**, no. 11, pp. 998–1007, 2012.

Umavathi, J.C., Liu, I.C., and Sheremet, M.A., Convective Heat Transfer in a Vertical Rectangular Duct Filled with a Nanofluid, *Heat Transf. Asian Res.*, vol. **44**, pp. 227–256, 2015.

Umavathi, J.C. and Mohite, M.B., Double-Diffusive Convective Transport in a Nanofluid-Saturated Porous Layer with Cross Diffusion and Variation of Viscosity and Conductivity, *Heat Transf. Asian Res.*, vol. **43**, pp. 628–652, 2014a.

Umavathi, J.C. and Mohite, M.B., The Onset of Convection in a Nanofluid Saturated Porous Layer Using Darcy Model with Cross Diffusion, *Meccanica*, vol. **49**, pp. 1159–1175, 2014b.

Umavathi, J.C. and Santosh, V., Non-Darcy Mixed Convection in a Vertical Porous Channel with Boundary Conditions of Third Kind, *Transp. Porous Media*, vol. **95**, pp. 111–131, 2012.

Umavathi, J.C. and Sheremet, M.A., Influence of Temperature Dependent Conductivity of a Nanofluid in a Vertical Rectangular Duct, *Int. J. Non Linear Mech.*, vol. **78**, pp. 17–28, 2016.